

Non-Hermitian ultra-strong bosonic condensation through interaction-induced caging

Mengjie Yang,^{1,2} Luqi Yuan,^{2,*} and Ching Hua Lee^{1,†}

¹*Department of Physics, National University of Singapore, Singapore 117551, Singapore*

²*State Key Laboratory of Advanced Optical Communication Systems and Networks, School of Physics and Astronomy, Shanghai Jiao Tong University, Shanghai 200240, China*

(Dated: October 3, 2024)

We uncover a new mechanism whereby the triple interplay of non-Hermitian pumping, bosonic interactions and nontrivial band topology leads to ultra-strong bosonic condensation. The extent of condensation goes beyond what is naively expected from the interaction-induced trapping of non-Hermitian pumped states, and is based on an emergent caging mechanism that can be further enhanced by topological boundary modes. Beyond our minimal model with 2 bosons, this caging remains applicable for generic many-boson systems subject to a broad range of density interactions and non-Hermitian hopping asymmetry. Our novel new mechanism for particle localization and condensation would inspire fundamental shifts in our comprehension of many-body non-Hermitian dynamics and opens new avenues for controlling and manipulating bosons.

Introduction.— In many-body physics, interactions between particles play a crucial role, driving interesting phenomena such as phase transitions [1–5], superconductivity [6–8], and quantum entanglement [5, 9–11]. Much of these physics can be observed through many-body dynamical simulations in both classical and quantum simulators [12–28].

There has been growing excitement surrounding the interplay between many-body interactions and the non-Hermitian skin effect (NHSE) [29–35]. This excitement stems from the non-locality and sensitivity of the NHSE, which has a profound impact on particle localization [36–42] and condensation dynamics [42–47], which can result in unexpected consequences when interplayed with quantum many-body interactions [29–35]. These include the emergence of a Fermi surface in a many-body non-Hermitian fermionic chain [29], exotic spin liquids from couplings to the environment [30], symmetry breaking and spectral structure of the interacting Hatano-Nelson model [31], and unconventional emission and absorption rates in non-Hermitian baths, as well as fundamental modifications of the quantum dynamics [32, 34]. Recently, the non-Hermitian Mott skin effect [48] has revealed the intriguing interplay between strong correlations and non-Hermitian topology in the many-body skin effect.

In this work, we uncovered a new mechanism whereby bosons can be made to condense very strongly through the triple interplay of non-Hermitian pumping, density interactions and non-trivial band topology. Due to the emergent non-locality of both the NHSE and the density interactions, the observed phenomenon is in stark contrast to the conventional behavior of interacting bosons, such as photons, which repel each other when they interact, leading to the quantum phenomenon known as photon blockade [49–52]. Our simulations show that ultra-

strong localization, and not just boundary state accumulation, is achieved when both non-Hermiticity and density interactions are present, which is not attainable by either alone.

Bosonic condensation from interactions and non-Hermiticity.— To demonstrate how non-Hermitian pumping, topology and bosonic interactions can interplay to cause unexpectedly strong bosonic condensation, we consider a minimal interacting 1D bosonic lattice model that contains topological edge modes at its boundary sites:

$$H = \sum_{x=1}^L t_L b_{2x-1}^\dagger b_{2x} + t_R b_{2x}^\dagger b_{2x-1} + \sum_{x=1}^{L-1} (b_{2x}^\dagger b_{2x+1} + b_{2x+1}^\dagger b_{2x}) + \frac{U}{2} n_{x_0}^2, \quad (1)$$

which is a Su-Schrieffer-Heeger (SSH) lattice [53] with asymmetric intercell (t_L and t_R) hoppings and unit intra-cell hoppings, equipped with a density interaction $\frac{1}{2}U n_{x_0}^2$ at site x_0 , $U \geq 0$. Here b_x (b_x^\dagger) is the bosonic annihilation (creation) operator at sites $x = 1, 2, \dots, 2L$, with $n_{x_0} = b_{x_0}^\dagger b_{x_0}$ the boson number operator. Non-Hermitian pumping [36–38, 40–42, 44, 47, 54–73] occurs towards the left if $r = t_L/t_R > 1$, accumulating the bosons towards the left boundary. However, when there are multiple indistinguishable bosons, this accumulation would also be affected by the repulsive ($U > 0$) interaction at site x_0 , with strength depending on bosonic occupancy. In this work, we have chosen the interaction $\frac{1}{2}U n_{x_0}^2$ that mimics the simplest possible nonlinearity in the mean-field limit, different from the usual Bose-Hubbard interaction [15, 49–52, 74] by a local density shift [75–79].

While one might naively expect a repulsive ($U > 0$) density interaction to suppress the NHSE accumulation primarily, the observed behavior can be dramatically different even with just two bosons. Two distinct measures of particle accumulation can be defined: the spatial density accumulation and the many-body correlation. An initial 2-boson state $|\phi(t=0)\rangle$ evolves according to the

* yuanluqi@sjtu.edu.cn

† phylch@nus.edu.sg

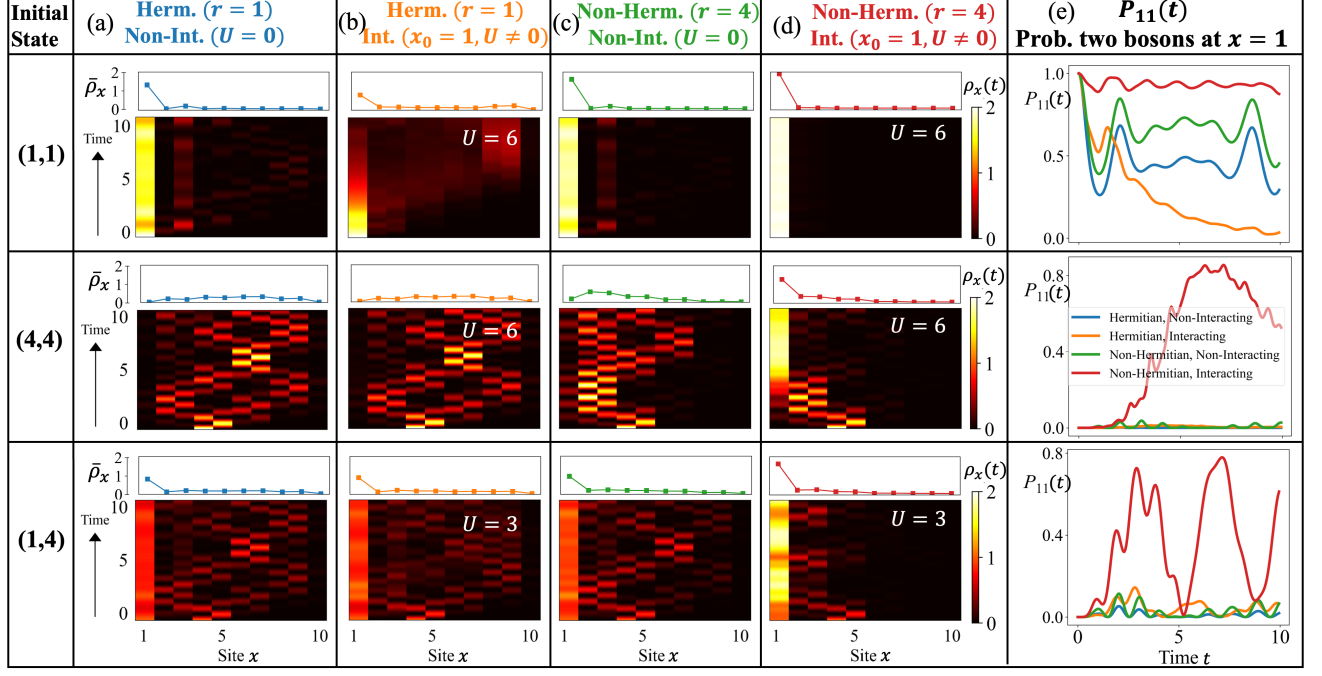


Figure 1. Spatial density accumulation (a-d) and ultra-strong bosonic condensation (e) due to a boundary density interaction at $x_0 = 1$, for different two-boson initial states $(1,1)$, $(4,4)$, and $(1,4)$ evolving via H [Eq. 1]. $r = 1$ or 4 corresponds to Hermitian (a,b) or non-Hermitian (c,d) cases, and $U = 0$ or $U \neq 0$ corresponds the absence (a,c) or presence (b,d) of the density interaction. (a-d) Heatmaps depict $\rho_x(t)$ [Eq. 3], the time-dependent boson number over the simulation duration $t \in [0, T]$ with $T = 10$. The line plot above each heatmap shows the corresponding time-averaged boson number profile $\bar{\rho}_i$ [Eq. 4]. The bosons are most likely to be trapped at site $x = 1$ in the presence of both leftwards NHSE ($r > 0$) and nonzero interaction ($U > 0$), as shown by the white and bright yellow regions in the heatmaps. While normally being considered as repulsive, the interaction term U also acts as a trap at $x_0 = 1$ in non-equilibrium dynamics. (e) The dramatic interplay of NHSE pumping and bosonic interaction is most saliently expressed through the bosonic condensation at $x = 1$, as given by the two-boson correlation P_{11} [Eq. 5]. Here, we observe significantly larger P_{11} , indicated by the red curves in all three (e) subfigures, which demonstrates the greatly enhanced ability to trap both bosons at site 1 when both $U > 0$ and $r > 0$.

Schrodinger equation $|\dot{\phi}(t)\rangle = -iH|\phi(t)\rangle$, and can be expressed as

$$|\phi(t)\rangle = \frac{1}{\sqrt{2}} \sum_{x=1}^{2L} \sum_{x'=1}^{2L} v_{xx'}(t) |(x, x')\rangle, \quad (2)$$

where $v_{xx'}(t) = v_{x'x}(t)$ is the amplitude of the basis state $|(x, x')\rangle = b_x^\dagger b_{x'}^\dagger |0\rangle$ containing indistinguishable bosons at sites x, x' . We define the 2-boson density at site $x = 1, 2, \dots, 2L$ by

$$\rho_x(t) = \frac{\langle \phi(t) | b_x^\dagger b_x | \phi(t) \rangle}{\langle \phi(t) | \phi(t) \rangle}, \quad (3)$$

with $0 \leq \rho_x(t) \leq 2$. Associated with it is the time averaged spatial density

$$\bar{\rho}_x = \frac{1}{T} \int_0^T \rho_x(t') dt', \quad (4)$$

where T is the simulation duration. While $\rho_x(t)$ and $\bar{\rho}_x$ reveal where the bosons localize on the lattice, a high value of $\rho_x(t)$ or $\bar{\rho}_x$ can physically arise either due to

strong single-boson localization at site x , or moderate double-boson condensation at the same site. To quantify this important distinction, we also examine the two-boson correlation probability

$$P_{xx'}(t) = \begin{cases} |v_{xx'}(t)|^2 & \text{if } x = x', \\ |\sqrt{2}v_{xx'}(t)|^2 & \text{if } x \neq x', \end{cases} \quad (5)$$

which represents the probability of observing a boson at sites x and x' at the same time t . For revealing underlying trends in the evolution of the two-boson correlation, we also define the time-smoothed correlation

$$\bar{P}_{xx'}(t) = \frac{1}{\Delta t} \int_{t-\Delta t}^t P_{xx'}(t') dt', \quad (6)$$

which removes temporal oscillations shorter than a prescribed timescale Δt .

We first consider scenarios where the density interaction is at the leftmost (boundary) site $x_0 = 1$. Figs. 1(a-d) showcase the evolution of the dynamical density $\rho_x(t)$ [Eq. 3] and its time-average $\bar{\rho}_x$ [Eq. 4] of three illustrative initial 2-boson state configurations. For the initial state $(1,1)$ (Top Row) where both bosons are already on

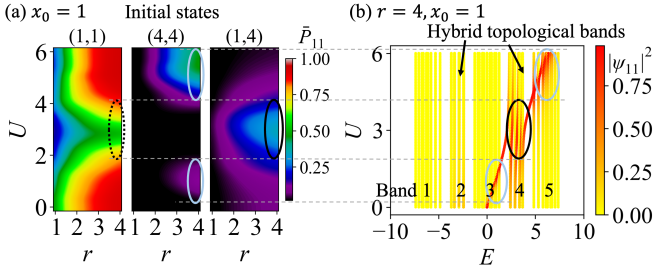


Figure 2. Extent of two-boson condensation due to a boundary density interaction at $x_0 = 1$ [Eq. 1], and its correspondence with the boundary localization of 2-boson spectral bands. (a) Time-averaged two-boson condensation probability \bar{P}_{11} [Eq. 6] at site $x = 1$, in the parameter space of non-Hermitian hopping asymmetry r and density interaction strength U . (b) Corresponding two-boson spectra at $r = 4$, which features five bands, with bands 2 and 4 being containing a pair of interaction-hybridized bulk and topological bosons. As U increases, it creates a group of eigenstates at $E \approx U$ that exhibits strong localization ψ_{11} (red) at $x = x_0 = 1$. Strong ψ_{11} localization in the hybrid topological band 4 leads to suppressed \bar{P}_{11} for the boundary-localized initial state $(1, 1)$ (circled in dashed black), but enhanced \bar{P}_{11} condensation for the initial state $(1, 4)$ (solid black). By contrast, strong ψ_{11} localization in the bulk bands 3 and 5 (circled in light blue) corresponds to enhanced \bar{P}_{11} for the bulk initial state $(4, 4)$.

$x_0 = 1$, the density interaction indeed repels the bosons in the Hermitian limit, as evidenced in the suppressed ρ_x density at $x = x_0 = 1$ across the Hermitian interacting vs. non-interacting cases (orange vs. blue). Somewhat expectedly, this suppression vanishes when the NHSE counteracts the repulsion by pumping the bosons towards $x_0 = 1$ (green and red). However, for the initial state $(4, 4)$ (Center Row) where both bosons are initially far from $x_0 = 1$, the boson density oscillates and spreads out, failing to accumulate appreciably at $x_0 = 1$ except when both the non-Hermiticity and interaction are present (red). Indeed, in this non-equilibrium scenario, the $U > 0$ density term behaves more like a local potential well that traps the $\rho_x(t)$ at $x = x_0$, rather than a repulsion. Qualitatively similar behavior is observed in the density evolution for initial state $(1, 4)$ (Bottom Row), when one of the bosons is initially already at $x_0 = 1$ and is as such unaffected by the NHSE.

What is striking, however, is the ultra-strong two-boson condensation at site $x_0 = 1$ when both non-Hermiticity ($r > 1$) and the density interaction ($U > 0$) are present. This is revealed in the dynamical $P_{11}(t)$ [Eq. 5] plots of Fig. 1(e), which shows the probability of both bosons condensing at $x = 1$. From the Top Row, when both bosons are prepared at $x = 1$ (initial state $=(1,1)$), they can only remain both there if non-Hermiticity and interaction are simultaneously present (red). But most surprising is what happens when at least one boson is initially away from $x = 1$ (Center and Bottom Rows): we observe *overwhelmingly* higher P_{11} only when non-Hermiticity and interaction simultaneously in-

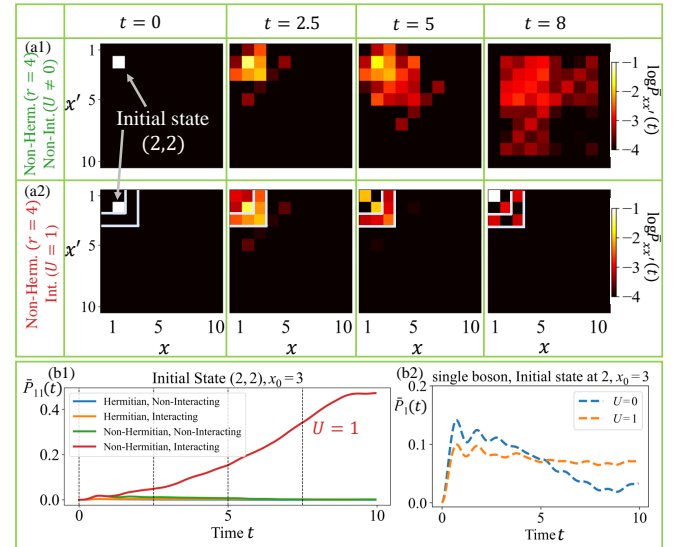


Figure 3. Caging mechanism of interaction term U with initial state $(2, 2)$, left of interaction position $x_0 = 3$. (a) Snapshots of smoothed time-averaged two-boson correlation probability \bar{P}_{11} (Eq. 6) at $t = 0, 2.5, 5, 8$ for (a1) NH non-interacting and (a2) NH interacting cases. An inverted L-shape indicates an effective interaction range. (b1) Probability of both bosons at site 1. NH interacting case (red) shows optimal trapping. (b2) Single-boson probability (\bar{P}_1) at site 1 for comparison. Surprisingly, the interaction term acts as a barrier, confining bosons to sites 1-3 in the NH interacting case, demonstrating a unique caging effect not observed in single-boson scenarios or non-interacting cases. This highlights the distinctive role of interactions in two-boson dynamics. Lattice: $L = 5$ cells; $U = 1$; hopping asymmetry $r = 4$; smoothing $\Delta t = 2$.

terplay (red), compared to having either on their own (yellow, green). This suggests that the ability to trap both bosons and suppress photon blockade [49–52] hinges on an emergent consequence of this interplay, a fact not evident from the density evolution alone [Fig. 1(a-d)].

To quantitatively characterize this two-boson condensation, we plot in Fig. 2(a) the time-averaged condensation probability $\bar{P}_{11} = \bar{P}_{11}(T)$ with $\Delta t = T$ [Eq. 6], which is the correlation P_{11} smoothed over the entire simulation duration T . The heatmap of \bar{P}_{11} in the interaction strength vs. non-Hermiticity U - r plane [Fig. 2(a)] reveals significantly enhanced \bar{P}_{11} (colored) for certain (U, r) regions, compared to the $r = 1$ Hermitian limit where \bar{P}_{11} essentially vanishes (black). While \bar{P}_{11} generally increases with r , optimal condensation \bar{P}_{11} occurs at windows of U that are highly dependent on the initial state, as will be explained below.

Topological origin of ultra-strong bosonic condensation.— Intriguingly, for a density interaction at the $x_0 = 1$ boundary, it turns out that the ultra-strong boundary bosonic condensation is not just due to the interaction-NHSE interplay, but also relies crucially on SSH topology. This is evident from the 2-boson band structure plot in Fig. 2(b), where each eigenenergy E is colored accord-

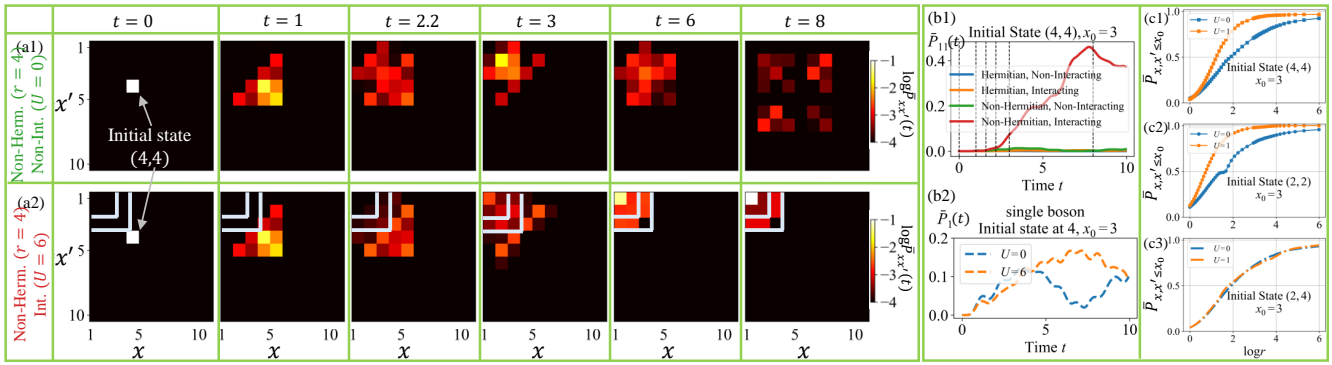


Figure 4. Caging mechanism of interaction term U with initial state $(4,4)$, right of interaction position $x_0 = 3$. (a) Snapshots of smoothed time-averaged two-boson correlation probability \bar{P}_{11} (Eq. 6) at $t = 0, 1, 1.6, 2.2, 3, 8$ for (a1) NH non-interacting and (a2) NH interacting cases. Initial similar behavior in both cases ($t = 0, 1$). Interaction barrier effect emerges ($t = 1.6, 2.2$). NHSE-assisted confinement to left side in interacting case ($t = 3, 8$). (b1) Smoothed probability of both bosons at site 1 (\bar{P}_1 in Eq. 6). (b2) Single-boson probability (\bar{P}_1) for comparison. Notably, the NH interacting case demonstrates superior trapping ability for two bosons compared to the single-boson scenario, highlighting a unique interplay between interaction and non-Hermiticity. $U = 6$ and smoothing $\Delta t = 2$. (c) Time-averaged two-boson probability \bar{P}_{mn} (Eq. 6) within the cage, $\sum m, n = 1^{x_0} \bar{P}_{mn}$, plotted against hopping asymmetry values $\log r \in [0, 6]$ for various initial states: (c1) $(4,4)$, (c2) $(2,2)$, and (c3) $(2,4)$. The orange curves ($U = 1$) in (c1) and (c2) confirm the caging mechanism. A slight deviation for the orange curve ($U = 1$) compared with the blue curve ($U = 0$) is observed in (c3), attributed to insufficient interaction time between the two bosons. Lattice size $L = 5$ unit cells.

ing to the overlap $\psi_{11} = \langle (1,1) | \psi \rangle$ of its corresponding eigenstate $|\psi\rangle$ with $|(1,1)\rangle = (b_1^\dagger)^2 |0\rangle$. Computed for our Hamiltonian H [Eq. 1] at strong non-Hermitian hopping asymmetry $r = 4$, it features 5 bands, with bands 2 and 4 arising from the hybridization of bulk and topological bands. This follows from the single-boson band structure [80], which contains two symmetrically gapped bulk bands separated by in-gap topological zero modes. The effect of the U density interaction is to induce high ψ_{11} overlap (red) successively from bands 3 to 5, as U is increased.

To illustrate, with the initial state $(1,1)$, suppressed \bar{P}_{11} at $U \approx 3$ corresponds to high ψ_{11} overlap with band 4 [circled in black in Figs. 2(a,b)]. This is because band 4 manifestly contain one bulk and one topological boson, which is not consistent with maintaining both bosons at $x_0 = 1$. As such, the same interaction strength of $U \approx 3$ leads to enhanced \bar{P}_{11} (dashed black) for the initial state $(1,4)$, where only one boson overlaps with the topological boundary mode. Likewise, $U \approx 1$ or $U \approx 5$ favors the \bar{P}_{11} bosonic condensation for the bulk initial state $(4,4)$, as circled in light blue, since the ψ_{11} overlap with the bulk bands (3 and 5) are strongest at these interaction strengths U .

2-boson interactions as caging mechanisms.— Interestingly, the boson density interaction can also act as a non-local cage when the interaction position x_0 is not at the boundary site 1. To demonstrate this, we shall show in Fig. 3 that, for an initial state with both bosons to the left of x_0 , an interaction U cages the evolved state, trapping it. And, more elaborately, we show in Fig. 4 that, for an initial state with both bosons to the right of x_0 , the interaction will first act as a barrier to the evolved state,

but will eventually still end up as a cage that traps the particle flux that leaked into it via NHSE pumping. We shall consider $x_0 = 3$ and initial states $(2,2)$ and $(4,4)$ in Fig. 3 and Fig. 4 respectively.

To illustrate the caging mechanism more intuitively, we express our 1D bosonic interacting model in its 2D configuration space (x, x') , where x and x' represent the positions of the two bosons. Here (x, x') and (x', x) refer to the same state due to bosonic statistics [74, 77, 81–84]. A key observation is that the nonlinear term $\frac{1}{2}U n_{x_0}^2$ can be interpreted as a non-local potential offset [74, 77].

When the initial state is already inside the cage, bosons are predominantly confined within the cage (inverted-L shape) between sites 1 and 3, as shown in Fig. 4(a2). This contrasts with Fig. 4(a1), which shows no such suppression of spreading, despite the pumping direction being towards the left-top corner. When the initial state is outside the cage, as in Fig. 4(a), bosons are pumped to the left side of the lattice due to skin pumping. However, once they enter the cage, they become trapped. This is clearly demonstrated in Fig. 4(a2) at $t = 3$ and $t = 8$, where bosons are predominantly confined to the left side of the lattice, explaining the prominence of the red curve in Fig. 4(b1).

To prove that this caging mechanism is unique to the interacting scenario and not merely a consequence of an effective on-site potential, we conducted a comparative analysis. We examined the probability (\bar{P}_1 , smoothed using the same method as in the two-boson case) of a single boson localized at the edge (site 1) of a 1D SSH chain with an on-site potential U at site 1. The single-boson case is not as effective as the two-boson case, as shown in Fig. 3(b2) and Fig. 4(b2), which stand in stark

contrast to the outstanding red curves in Fig. 3(b1) and Fig. 4(b1). This further proves that the interaction effect is unique to the two-boson case.

The efficacy of the caging mechanism is corroborated by analyzing the time-averaged two-boson probability within the caging region, $\sum_{m,n=1}^{x_0} \bar{P}_{mn}$, as a function of hopping asymmetry $\log r$ for diverse initial states (Fig. 4(c)) in long-time dynamics over a period of 500. In Fig. 4(c1) and (c2), the significantly higher values of the interacting case ($U = 1$, orange curves) compared to the non-interacting case ($U = 0$, blue curves) provide strong evidence for the caging phenomenon. Notably, Fig. 4(c3) exhibits a small deviation between the interacting and non-interacting scenarios, which we attribute to limited interaction time between the bosons when they start on opposite sides of the interaction site. This leads to a less pronounced caging effect, as the boson starting on site 2 is less likely to occupy site 3 due to the leftward skin pumping. This observation also explains the small difference between orange and blue curves in Fig. 3(b2) and Fig. 4(b2) – the caging effect is significant only when two bosons are interacting.

Conclusion.— To summarize, our investigation has revealed how the intriguing interplay between NHSE, topology and boson-boson interactions can unexpectedly

lead to ultra-strong edge condensation of the bosons. The extent of this particle condensation goes beyond intuitive expectations of NHSE-pumped bosons trapped by the interaction, being also facilitated by the interaction-induced hybridization of topological and bulk states. Moreover, even more pronounced bosonic condensation can be induced by density interactions in the bulk ($x_0 \neq 1$) due to an emergent caging mechanism. This trapping phenomenon is not observed in single-boson dynamics, and generalizes to higher numbers of bosons as well as generic density interactions that are non-local in the many-body configuration space. Our findings provide new perspectives on the role of interactions in the condensation and localization of bosons in non-Hermitian topological systems, offering a novel approach to trapping and controlling bosons. Our results are not limited to the specific model we have studied but can be extended to other systems with different forms of interactions and topologies. Experimentally, various platforms can potentially implement the setup for locally interacting bosons, including optical lattices [18, 85–89], photonic systems [75, 90–95], and circuit QED [25, 96–99]. Specifically, we have a potential experimental realization of the bosonic interacting model using resonator arrays in real space in the Supplemental Material [80].

Supplemental Material for “Non-Hermitian ultra-strong bosonic condensation through interaction-induced caging”

S1. SINGLE-BOSON AND TWO-BOSON SPECTRA

In the main text, we have computed for our Hamiltonian H [Eq. 1 in the main text] for two bosons at strong non-Hermitian hopping asymmetry $r = 4$. The emergence of five distinct bands in the two-boson spectrum, compared to three bands typically seen in single-boson cases, requires careful explanation. Below, we elucidate the existence of these five bands by analyzing the system in the non-interacting limit ($U \rightarrow 0$).

The single-boson band structure, shown in Fig. S1(a), contains two symmetrically gapped bulk bands (E_1 and E_2) separated by in-gap topological zero modes (E_0). The corresponding eigenstates demonstrate distinct localization patterns, with extended states for bulk bands [Fig. S1(b)] and localized states for zero modes [Fig. S1(c)].

For the two-boson case in the non-interacting limit, the energy spectrum can be systematically constructed through all possible pairwise combinations of the single-particle energies. As shown in Fig. S2(a), this results in five distinct bands rather than three. The lowest [band 1 in Fig. S2] and highest [band 5 in Fig. S2] bands correspond to configurations where both bosons occupy the lower ($E_1 \oplus E_1$) or upper ($E_2 \oplus E_2$) bulk bands, respectively. The intermediate bands 2 and 4 in Fig. S2 arise from mixed occupations, where one boson occupies the zero mode while the other occupies either the lower ($E_0 \oplus E_1$) or upper ($E_0 \oplus E_2$) bulk band.

Notably, the central band [band 3 in Fig. S2] emerges from the hybridization of two distinct configurations: one where the bosons are distributed between the lower and upper bulk bands ($E_1 \oplus E_2$), and another where both bosons occupy the zero mode ($E_0 \oplus E_0$). This hybridization explains why we observe five bands rather than six possible energy combinations, as the energetic proximity of these configurations leads to their mixing into a single hybridized band.

The localization patterns shown in Fig. S2(b) and (c) reflect this hybridization, exhibiting characteristics that can be understood as superpositions of the single-particle localization patterns.

S2. POSSIBLE EXPERIMENTAL REALIZATION

In the main text, we have proposed a bosonic interacting model in a non-Hermitian SSH lattice, as shown in

Eq. S1. The Hamiltonian is

$$H = \sum_{x=1}^L t_L b_{2x-1}^\dagger b_{2x} + t_R b_{2x}^\dagger b_{2x-1} + \sum_{x=1}^{L-1} (b_{2x}^\dagger b_{2x+1} + b_{2x+1}^\dagger b_{2x}) + \frac{U}{2} n_{x_0}^2, \quad (\text{S1})$$

Various physical platforms have experimentally realized non-Hermitian systems, including mature mechanical platforms [100–103], photonic platforms [45, 104–107], electrical circuit platforms [61, 108–120], and quantum circuit platforms [13, 121–130]. In the meantime, multi-boson physics can be explored using cold atoms in optical lattices [15–19], photonic waveguide arrays [131–138], and superconducting circuits [25–28].

Below, we propose a potential experimental realization of the bosonic interacting model, as presented in Eq. S1, using resonator arrays in real space.

Arrays of micro-resonators have been extensively utilized to implement one-dimensional (1D) and two-dimensional (2D) photonic lattices, particularly in the investigation of non-Hermitian photonics over the past decade [139–144]. These designs predominantly employ ring resonators, which can achieve exceptionally high Q factors [144].

It is noted that in Ref. [105], the authors demonstrate a feasible design of a one-dimensional non-Hermitian Su-Schrieffer-Heeger model based on photonic coupled resonant arrays in Fig. S3. The non-Hermitian asymmetric coupling can be realized by the judicious design of optical gain and loss elements into unidirectional coupling link rings, as shown in Fig. S3(b). The corresponding Hamiltonian is [105]

$$H(k) = \begin{pmatrix} 0 & t_1 - \frac{\gamma}{2} + t_2 e^{ik} \\ t_1 + \frac{\gamma}{2} + t_2 e^{-ik} & 0 \end{pmatrix}. \quad (\text{S2})$$

Here, in their model, the hopping amplitudes $t_1 \pm \gamma$ and t_2 correspond to intracell hoppings t_L, t_R and intercell hopping (where we have set to be 1 for simplicity) in our model in Eq. S1, respectively. The non-Hermitian skin effect is observed in their model, which is consistent with our results.

Based on the design in Ref. [105], we only need the nonlinearity to be implemented in the system. The Kerr effect in the micro-resonators can introduce the nonlinearity. The Kerr effect, i.e., the third-order nonlinearity $\chi^{(3)}$, is a nonlinear optical effect that occurs when the refractive index of a material changes with the intensity of light.

The third-order nonlinearity can be achieved through natural materials (although the $\chi^{(3)}$ value is relatively

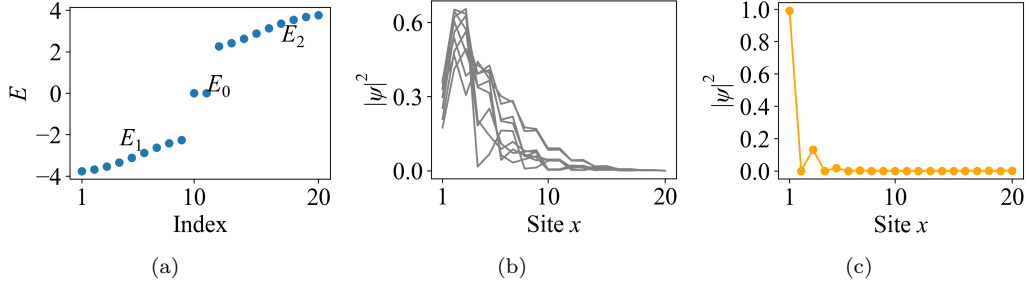


Figure S1. Single-boson spectrum of the SSH model. (a) The energy spectrum shows two bulk bands (E_1 and E_2) separated by topological zero modes (E_0). (b) Localization pattern $|\psi|^2$ of extended states in the bulk bands. (c) Localization of the topological zero mode, showing edge confinement.

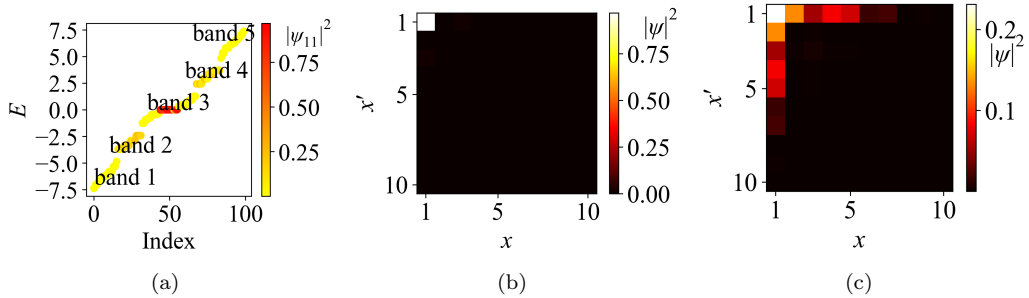


Figure S2. Two-boson spectrum in the non-interacting limit ($U = 0$). (a) Energy spectrum showing five bands arising from combinations of single-particle energies. Band 1 results from hybridization of $E_1 \oplus E_1$. Band 2 results from hybridization of $E_1(E_0) \oplus E_0(E_1)$. Band 3 results from hybridization of $E_1 \oplus E_2$ and $E_0 \oplus E_0$ configurations. Band 4 results from hybridization of $E_2(E_0) \oplus E_0(E_2)$. Band 5 results from hybridization of $E_2 \oplus E_2$. (b) Localization pattern of a zero-corner state in band 3. (c) Localization of mixed bulk-topological states in bands 2 and 4.

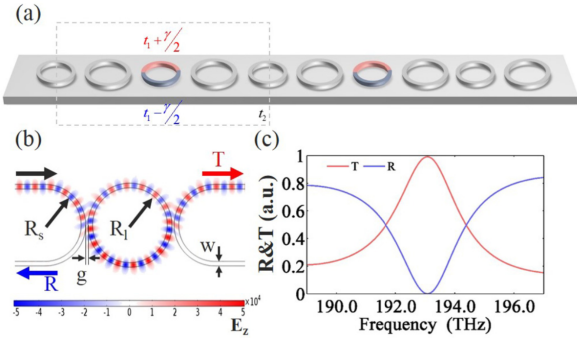


Figure S3. Schematic of the photonic coupled resonator arrays for realizing the non-Hermitian SSH model. The judicious design of optical gain and loss elements into unidirectional coupling link rings realise the non-Hermitian asymmetric coupling coupling coupling. This figure is adapted from Ref. [105].

small) or by employing cavity QED based on electromagnetically induced transparency (EIT) to achieve an equivalent $\chi^{(3)}$. The latter involves introducing atoms [79, 145–147] or quantum dots into a cavity [49, 148–151], and through appropriate external field control, inducing a target optical field with strong effective nonlinearity. Additionally, the versatility of synthetic dimensions provides opportunities to implement the nonlinear term $\frac{U}{2}n_{x_0}^2$ in Eq. S1 demonstrated in Eq. (14) in Ref. [78].

[1] S. Murphy, J. Eisenstein, G. Boebinger, L. Pfeiffer, and K. West, Many-body integer quantum hall effect: evidence for new phase transitions, *Physical review letters* **72**, 728 (1994).
[2] S. Diehl, A. Tomadin, A. Micheli, R. Fazio, and P. Zoller, Dynamical phase transitions and instabilities

in open atomic many-body systems, *Physical review letters* **105**, 015702 (2010).

[3] M. Serbyn, Z. Papić, and D. A. Abanin, Criterion for many-body localization-delocalization phase transition, *Physical Review X* **5**, 041047 (2015).

[4] P. Jurcevic, H. Shen, P. Hauke, C. Maier, T. Brydges, C. Hempel, B. Lanyon, M. Heyl, R. Blatt, and C. Roos, Direct observation of dynamical quantum phase transitions in an interacting many-body system, *Physical review letters* **119**, 080501 (2017).

[5] D. A. Abanin, E. Altman, I. Bloch, and M. Serbyn, Colloquium: Many-body localization, thermalization, and entanglement, *Reviews of Modern Physics* **91**, 021001 (2019).

[6] M. L. Kiesel, C. Platt, W. Hanke, D. A. Abanin, and R. Thomale, Competing many-body instabilities and unconventional superconductivity in graphene, *Physical Review B* **86**, 020507 (2012).

[7] C. Eichler, J. Mlynek, J. Butscher, P. Kurpiers, K. Hammerer, T. J. Osborne, and A. Wallraff, Exploring interacting quantum many-body systems by experimentally creating continuous matrix product states in superconducting circuits, *Physical Review X* **5**, 041044 (2015).

[8] K. Xu, J.-J. Chen, Y. Zeng, Y.-R. Zhang, C. Song, W. Liu, Q. Guo, P. Zhang, D. Xu, H. Deng, *et al.*, Emulating many-body localization with a superconducting quantum processor, *Physical review letters* **120**, 050507 (2018).

[9] L. Amico, R. Fazio, A. Osterloh, and V. Vedral, Entanglement in many-body systems, *Reviews of modern physics* **80**, 517 (2008).

[10] N. Laflorencie, Quantum entanglement in condensed matter systems, *Physics Reports* **646**, 1 (2016).

[11] D.-L. Deng, X. Li, and S. D. Sarma, Quantum entanglement in neural network states, *Physical Review X* **7**, 021021 (2017).

[12] M. J. Hartmann and G. Carleo, Neural-network approach to dissipative quantum many-body dynamics, *Physical review letters* **122**, 250502 (2019).

[13] A. Smith, M. Kim, F. Pollmann, and J. Knolle, Simulating quantum many-body dynamics on a current digital quantum computer, *npj Quantum Information* **5**, 106 (2019).

[14] M. Schmitt and M. Heyl, Quantum many-body dynamics in two dimensions with artificial neural networks, *Physical Review Letters* **125**, 100503 (2020).

[15] D. Jaksch, C. Bruder, J. I. Cirac, C. W. Gardiner, and P. Zoller, Cold bosonic atoms in optical lattices, *Physical Review Letters* **81**, 3108 (1998).

[16] R. Grimm, M. Weidemüller, and Y. B. Ovchinnikov, Optical dipole traps for neutral atoms, in *Advances in atomic, molecular, and optical physics*, Vol. 42 (Elsevier, 2000) pp. 95–170.

[17] I. Bloch, J. Dalibard, and W. Zwerger, Many-body physics with ultracold gases, *Reviews of modern physics* **80**, 885 (2008).

[18] C. Chin, R. Grimm, P. Julienne, and E. Tiesinga, Feshbach resonances in ultracold gases, *Reviews of Modern Physics* **82**, 1225 (2010).

[19] L. Zeng and J. Zeng, Gap-type dark localized modes in a bose-einstein condensate with optical lattices, *Advanced Photonics* **1**, 046004 (2019).

[20] P. N. Jepsen, J. Amato-Grill, I. Dimitrova, W. W. Ho, E. Demler, and W. Ketterle, Spin transport in a tunable heisenberg model realized with ultracold atoms, *Nature* **588**, 403 (2020).

[21] S. Scherg, T. Kohlert, P. Sala, F. Pollmann, B. Hebbe Madhusudhana, I. Bloch, and M. Aidelsburger, Observing non-ergodicity due to kinetic constraints in tilted fermi-hubbard chains, *Nature Communications* **12**, 4490 (2021).

[22] P. Zhang, H. Dong, Y. Gao, L. Zhao, J. Hao, J.-Y. Desaules, Q. Guo, J. Chen, J. Deng, B. Liu, *et al.*, Many-body hilbert space scarring on a superconducting processor, *Nature Physics* **19**, 120 (2023).

[23] H. Bernien, S. Schwartz, A. Keesling, H. Levine, A. Omran, H. Pichler, S. Choi, A. S. Zibrov, M. Endres, M. Greiner, *et al.*, Probing many-body dynamics on a 51-atom quantum simulator, *Nature* **551**, 579 (2017).

[24] D. Bluvstein, A. Omran, H. Levine, A. Keesling, G. Semeghini, S. Ebadi, T. T. Wang, A. A. Michailidis, N. Maskara, W. W. Ho, *et al.*, Controlling quantum many-body dynamics in driven rydberg atom arrays, *Science* **371**, 1355 (2021).

[25] M. H. Devoret and R. J. Schoelkopf, Superconducting circuits for quantum information: an outlook, *Science* **339**, 1169 (2013).

[26] X. Gu, S. Chen, and Y.-x. Liu, Topological edge states and pumping in a chain of coupled superconducting qubits, *arXiv preprint arXiv:1711.06829* (2017).

[27] Z. Yan, Y.-R. Zhang, M. Gong, Y. Wu, Y. Zheng, S. Li, C. Wang, F. Liang, J. Lin, Y. Xu, *et al.*, Strongly correlated quantum walks with a 12-qubit superconducting processor, *Science* **364**, 753 (2019).

[28] Y. Yanay, J. Braumüller, S. Gustavsson, W. D. Oliver, and C. Tahan, Two-dimensional hard-core bose-hubbard model with superconducting qubits, *npj Quantum Information* **6**, 58 (2020).

[29] S. Mu, C. H. Lee, L. Li, and J. Gong, Emergent fermi surface in a many-body non-hermitian fermionic chain, *Physical Review B* **102**, 081115 (2020).

[30] K. Yang, S. C. Morampudi, and E. J. Bergholtz, Exceptional spin liquids from couplings to the environment, *Physical Review Letters* **126**, 077201 (2021).

[31] S.-B. Zhang, M. M. Denner, T. Bzdušek, M. A. Sentef, and T. Neupert, Symmetry breaking and spectral structure of the interacting hatano-nelson model, *Physical Review B* **106**, L121102 (2022).

[32] Z. Gong, M. Bello, D. Malz, and F. K. Kunst, Anomalous behaviors of quantum emitters in non-hermitian baths, *Physical Review Letters* **129**, 223601 (2022).

[33] K. Kawabata, K. Shiozaki, and S. Ryu, Many-body topology of non-hermitian systems, *Physical Review B* **105**, 165137 (2022).

[34] F. Roccati, S. Lorenzo, G. Calajò, G. M. Palma, A. Carollo, and F. Ciccarello, Exotic interactions mediated by a non-hermitian photonic bath, *Optica* **9**, 565 (2022).

[35] F. Qin, R. Shen, C. H. Lee, *et al.*, Non-hermitian squeezed polarons, *Physical Review A* **107**, L010202 (2023).

[36] T. E. Lee, Anomalous edge state in a non-hermitian lattice, *Physical review letters* **116**, 133903 (2016).

[37] S. Yao and Z. Wang, Edge states and topological invariants of non-hermitian systems, *Physical review letters* **121**, 086803 (2018).

[38] C. H. Lee and R. Thomale, Anatomy of skin modes and topology in non-hermitian systems, *Physical Review B* **99**, 201103 (2019).

[39] Y. Ashida, Z. Gong, and M. Ueda, Non-hermitian physics, *Advances in Physics* **69**, 249 (2020).

[40] L. Li, C. H. Lee, S. Mu, and J. Gong, Critical non-hermitian skin effect, *Nature communications* **11**, 5491 (2020).

[41] M. Yang, L. Wang, X. Wu, H. Xiao, D. Yu, L. Yuan, and X. Chen, Concentrated subradiant modes in a one-dimensional atomic array coupled with chiral waveguides, *Physical Review A* **106**, 043717 (2022).

[42] R. Lin, T. Tai, L. Li, and C. H. Lee, Topological non-hermitian skin effect, *Frontiers of Physics* **18**, 53605 (2023).

[43] S. Longhi, Unraveling the non-hermitian skin effect in dissipative systems, *Physical Review B* **102**, 201103 (2020).

[44] F. Song, S. Yao, and Z. Wang, Non-hermitian skin effect and chiral damping in open quantum systems, *Physical review letters* **123**, 170401 (2019).

[45] L. Xiao, T. Deng, K. Wang, G. Zhu, Z. Wang, W. Yi, and P. Xue, Non-hermitian bulk-boundary correspondence in quantum dynamics, *Nature Physics* **16**, 761 (2020).

[46] Q. Liang, D. Xie, Z. Dong, H. Li, H. Li, B. Gadway, W. Yi, and B. Yan, Dynamic signatures of non-hermitian skin effect and topology in ultracold atoms, *Physical review letters* **129**, 070401 (2022).

[47] M. Yang and C. H. Lee, Percolation-induced \mathcal{PT} symmetry breaking, *Phys. Rev. Lett.* **133**, 136602 (2024).

[48] T. Yoshida, S.-B. Zhang, T. Neupert, and N. Kawakami, Non-hermitian mott skin effect, *Physical Review Letters* **133**, 076502 (2024).

[49] K. M. Birnbaum, A. Boca, R. Miller, A. D. Boozer, T. E. Northup, and H. J. Kimble, Photon blockade in an optical cavity with one trapped atom, *Nature* **436**, 87 (2005).

[50] P. Rabl, Photon blockade effect in optomechanical systems, *Physical review letters* **107**, 063601 (2011).

[51] A. Ridolfo, M. Leib, S. Savasta, and M. J. Hartmann, Photon blockade in the ultrastrong coupling regime, *Physical review letters* **109**, 193602 (2012).

[52] R. Huang, A. Miranowicz, J.-Q. Liao, F. Nori, and H. Jing, Nonreciprocal photon blockade, *Physical review letters* **121**, 153601 (2018).

[53] W. Su, J. Schrieffer, and A. J. Heeger, Solitons in polyacetylene, *Physical review letters* **42**, 1698 (1979).

[54] V. M. Alvarez, J. B. Vargas, and L. F. Torres, Non-hermitian robust edge states in one dimension: Anomalous localization and eigenspace condensation at exceptional points, *Physical Review B* **97**, 121401 (2018).

[55] F. K. Kunst, E. Edvardsson, J. C. Budich, and E. J. Bergholtz, Biorthogonal bulk-boundary correspondence in non-hermitian systems, *Physical review letters* **121**, 026808 (2018).

[56] N. Okuma, K. Kawabata, K. Shiozaki, and M. Sato, Topological origin of non-hermitian skin effects, *Physical review letters* **124**, 086801 (2020).

[57] N. Okuma and M. Sato, Non-hermitian topological phenomena: A review, *Annual Review of Condensed Matter Physics* **14**, 83 (2023).

[58] S. Longhi, Topological phase transition in non-hermitian quasicrystals, *Physical review letters* **122**, 237601 (2019).

[59] K. Kawabata, K. Shiozaki, M. Ueda, and M. Sato, Symmetry and topology in non-hermitian physics, *Physical Review X* **9**, 041015 (2019).

[60] C. H. Lee, L. Li, and J. Gong, Hybrid higher-order skin-topological modes in nonreciprocal systems, *Physical review letters* **123**, 016805 (2019).

[61] T. Helbig, T. Hofmann, S. Imhof, M. Abdelghany, T. Kiessling, L. Molenkamp, C. Lee, A. Szameit, M. Greiter, and R. Thomale, Generalized bulk-boundary correspondence in non-hermitian topoelectrical circuits, *Nature Physics* **16**, 747 (2020).

[62] W.-T. Xue, Y.-M. Hu, F. Song, and Z. Wang, Non-hermitian edge burst, *Physical Review Letters* **128**, 120401 (2022).

[63] C. H. Lee, L. Li, R. Thomale, and J. Gong, Unraveling non-hermitian pumping: emergent spectral singularities and anomalous responses, *Physical Review B* **102**, 085151 (2020).

[64] D. Zou, T. Chen, W. He, J. Bao, C. H. Lee, H. Sun, and X. Zhang, Observation of hybrid higher-order skin-topological effect in non-hermitian topoelectrical circuits, *Nature Communications* **12**, 7201 (2021).

[65] X. Zhang, Y. Tian, J.-H. Jiang, M.-H. Lu, and Y.-F. Chen, Observation of higher-order non-hermitian skin effect, *Nature communications* **12**, 5377 (2021).

[66] L. Li and C. H. Lee, Non-hermitian pseudo-gaps, *Science Bulletin* **67**, 685 (2022).

[67] S. Longhi, Self-healing of non-hermitian topological skin modes, *Physical Review Letters* **128**, 157601 (2022).

[68] Z. Gu, H. Gao, H. Xue, J. Li, Z. Su, and J. Zhu, Transient non-hermitian skin effect, *Nature Communications* **13**, 7668 (2022).

[69] R. Shen and C. H. Lee, Non-hermitian skin clusters from strong interactions, *Communications Physics* **5**, 238 (2022).

[70] H. Jiang and C. H. Lee, Dimensional transmutation from non-hermiticity, *Physical Review Letters* **131**, 076401 (2023).

[71] T. Tai and C. H. Lee, Zoology of non-hermitian spectra and their graph topology, *Physical Review B* **107**, L220301 (2023).

[72] S. Longhi, Non-bloch-band collapse and chiral zener tunneling, *Physical review letters* **124**, 066602 (2020).

[73] Q. Lin, T. Li, L. Xiao, K. Wang, W. Yi, and P. Xue, Observation of non-hermitian topological anderson insulator in quantum dynamics, *Nature Communications* **13**, 3229 (2022).

[74] K. Winkler, G. Thalhammer, F. Lang, R. Grimm, J. Hecker Denschlag, A. Daley, A. Kantian, H. Büchler, and P. Zoller, Repulsively bound atom pairs in an optical lattice, *Nature* **441**, 853 (2006).

[75] H. Xiao, L. Wang, Z.-H. Li, X. Chen, and L. Yuan, Bound state in a giant atom-modulated resonators system, *npj Quantum Information* **8**, 80 (2022).

[76] L. Yuan, A. Dutt, M. Qin, S. Fan, and X. Chen, Creating locally interacting hamiltonians in the synthetic frequency dimension for photons, *Photonics Research* **8**, B8 (2020).

[77] D. Cheng, B. Peng, D.-W. Wang, X. Chen, L. Yuan, and S. Fan, Arbitrary synthetic dimensions via multiboson dynamics on a one-dimensional lattice, *Physical Review Research* **3**, 033069 (2021).

[78] L. Barbiero, L. Chomaz, S. Nascimbene, and N. Goldman, Bose-hubbard physics in synthetic dimensions from interaction trotterization, *Physical Review Research* **2**, 043340 (2020).

[79] D. E. Chang, V. Vuletić, and M. D. Lukin, Quantum nonlinear optics—photon by photon, *Nature Photonics* **8**, 685 (2014).

[80] See supplemental material.

[81] M. Valiente and D. Petrosyan, Two-particle states in the hubbard model, *Journal of Physics B: Atomic, Molecular and Optical Physics* **41**, 161002 (2008).

[82] M. Di Liberto, A. Recati, I. Carusotto, and C. Menotti, Two-body physics in the su-schrieffer-heeger model, *Physical Review A* **94**, 062704 (2016).

[83] M. A. Gorlach and A. N. Poddubny, Topological edge states of bound photon pairs, *Physical Review A* **95**, 053866 (2017).

[84] C. H. Lee, Many-body topological and skin states without open boundaries, *Physical Review B* **104**, 195102 (2021).

[85] O. Mandel, M. Greiner, A. Widera, T. Rom, T. W. Hänsch, and I. Bloch, Controlled collisions for multi-particle entanglement of optically trapped atoms, *Nature* **425**, 937 (2003).

[86] P. Lee, M. Anderlini, B. Brown, J. Sebby-Strabley, W. Phillips, and J. Porto, Sublattice addressing and spin-dependent motion of atoms in a double-well lattice, *Physical Review Letters* **99**, 020402 (2007).

[87] P. Soltan-Panahi, J. Struck, P. Hauke, A. Bick, W. Plenkers, G. Meineke, C. Becker, P. Windpassinger, M. Lewenstein, and K. Sengstock, Multi-component quantum gases in spin-dependent hexagonal lattices, *Nature Physics* **7**, 434 (2011).

[88] A. Kaufman, B. Lester, M. Foss-Feig, M. Wall, A. Rey, and C. Regal, Entangling two transportable neutral atoms via local spin exchange, *Nature* **527**, 208 (2015).

[89] Q.-Y. Liang, A. V. Venkatramani, S. H. Cantu, T. L. Nicholson, M. J. Gullans, A. V. Gorshkov, J. D. Thompson, C. Chin, M. D. Lukin, and V. Vuletić, Observation of three-photon bound states in a quantum nonlinear medium, *Science* **359**, 783 (2018).

[90] A. Szameit, I. L. Garanovich, M. Heinrich, A. A. Sukhorukov, F. Dreisow, T. Pertsch, S. Nolte, A. Tünnermann, and Y. S. Kivshar, Observation of defect-free surface modes in optical waveguide arrays, *Physical review letters* **101**, 203902 (2008).

[91] N. K. Efremidis, S. Sears, D. N. Christodoulides, J. W. Fleischer, and M. Segev, Discrete solitons in photorefractive optically induced photonic lattices, *Physical Review E* **66**, 046602 (2002).

[92] T. Meany, M. Gräfe, R. Heilmann, A. Perez-Leija, S. Gross, M. J. Steel, M. J. Withford, and A. Szameit, Laser written circuits for quantum photonics, *Laser & Photonics Reviews* **9**, 363 (2015).

[93] M. Notomi, E. Kuramochi, and T. Tanabe, Large-scale arrays of ultrahigh-q coupled nanocavities, *Nature photonics* **2**, 741 (2008).

[94] B. Corcoran, C. Monat, M. Pelusi, C. Grillet, T. White, L. O’Faolain, T. F. Krauss, B. J. Eggleton, and D. J. Moss, Optical signal processing on a silicon chip at 640gb/s using slow-light, *Optics express* **18**, 7770 (2010).

[95] K. Nozaki, A. Shinya, S. Matsuo, T. Sato, E. Kuramochi, and M. Notomi, Ultralow-energy and high-contrast all-optical switch involving fano resonance based on coupled photonic crystal nanocavities, *Optics express* **21**, 11877 (2013).

[96] A. A. Houck, H. E. Türeci, and J. Koch, On-chip quantum simulation with superconducting circuits, *Nature Physics* **8**, 292 (2012).

[97] T. Hime, P. Reichardt, B. Plourde, T. Robertson, C.-E. Wu, A. Ustinov, and J. Clarke, Solid-state qubits with current-controlled coupling, *science* **314**, 1427 (2006).

[98] M. Pechal, S. Berger, A. Abdumalikov Jr, J. Fink, J. A. Mlynek, L. Steffen, A. Wallraff, and S. Filipp, Geometric phase and nonadiabatic effects in an electronic harmonic oscillator, *Physical Review Letters* **108**, 170401 (2012).

[99] S. Filipp, P. Maurer, P. J. Leek, M. Baur, R. Bianchetti, J. Fink, M. Göppl, L. Steffen, J. M. Gambetta, A. Blais, *et al.*, Two-qubit state tomography using a joint dispersive readout, *Physical review letters* **102**, 200402 (2009).

[100] M. Brandenbourger, X. Locsin, E. Lerner, and C. Coulais, Non-reciprocal robotic metamaterials, *Nature communications* **10**, 4608 (2019).

[101] A. Ghatak, M. Brandenbourger, J. Van Wezel, and C. Coulais, Observation of non-hermitian topology and its bulk–edge correspondence in an active mechanical metamaterial, *Proceedings of the National Academy of Sciences* **117**, 29561 (2020).

[102] X. Wen, X. Zhu, A. Fan, W. Y. Tam, J. Zhu, H. W. Wu, F. Lemoult, M. Fink, and J. Li, Unidirectional amplification with acoustic non-hermitian space- time varying metamaterial, *Communications physics* **5**, 18 (2022).

[103] H. Xiu, I. Frankel, H. Liu, K. Qian, S. Sarkar, B. MacNider, Z. Chen, N. Boechler, and X. Mao, Synthetically non-hermitian nonlinear wave-like behavior in a topological mechanical metamaterial, *Proceedings of the National Academy of Sciences* **120**, e2217928120 (2023).

[104] M. Pan, H. Zhao, P. Miao, S. Longhi, and L. Feng, Photonic zero mode in a non-hermitian photonic lattice, *Nature communications* **9**, 1308 (2018).

[105] X. Zhu, H. Wang, S. K. Gupta, H. Zhang, B. Xie, M. Lu, and Y. Chen, Photonic non-hermitian skin effect and non-bloch bulk-boundary correspondence, *Physical Review Research* **2**, 013280 (2020).

[106] Y. Song, W. Liu, L. Zheng, Y. Zhang, B. Wang, and P. Lu, Two-dimensional non-hermitian skin effect in a synthetic photonic lattice, *Physical Review Applied* **14**, 064076 (2020).

[107] Y. Ao, X. Hu, Y. You, C. Lu, Y. Fu, X. Wang, and Q. Gong, Topological phase transition in the non-hermitian coupled resonator array, *Physical Review Letters* **125**, 013902 (2020).

[108] T. Hofmann, T. Helbig, C. H. Lee, M. Greiter, and R. Thomale, Chiral voltage propagation and calibration in a topoelectrical chern circuit, *Physical review letters* **122**, 247702 (2019).

[109] M. Ezawa, Electric circuits for non-hermitian chern insulators, *Physical Review B* **100**, 081401 (2019).

[110] T. Hofmann, T. Helbig, F. Schindler, N. Salgo, M. Brzezińska, M. Greiter, T. Kiessling, D. Wolf, A. Vollhardt, A. Kabaši, *et al.*, Reciprocal skin effect and its realization in a topoelectrical circuit, *Physical Review Research* **2**, 023265 (2020).

[111] S. Liu, S. Ma, C. Yang, L. Zhang, W. Gao, Y. J. Xiang, T. J. Cui, and S. Zhang, Gain-and loss-induced topological insulating phase in a non-hermitian electrical circuit, *Physical Review Applied* **13**, 014047 (2020).

[112] S. Liu, R. Shao, S. Ma, L. Zhang, O. You, H. Wu, Y. J. Xiang, T. J. Cui, and S. Zhang, Non-hermitian skin effect in a non-hermitian electrical circuit, *Research*

(2021).

[113] A. Stegmaier, S. Imhof, T. Helbig, T. Hofmann, C. H. Lee, M. Kremer, A. Fritzsche, T. Feichtner, S. Klembt, S. Höfling, *et al.*, Topological defect engineering and p t symmetry in non-hermitian electrical circuits, *Physical Review Letters* **126**, 215302 (2021).

[114] X.-X. Zhang and M. Franz, Non-hermitian exceptional landau quantization in electric circuits, *Physical Review Letters* **124**, 046401 (2020).

[115] X. Zhang, B. Zhang, W. Zhao, and C. H. Lee, Observation of non-local impedance response in a passive electrical circuit, *arXiv preprint arXiv:2211.09152* (2022).

[116] C. Shang, S. Liu, R. Shao, P. Han, X. Zang, X. Zhang, K. N. Salama, W. Gao, C. H. Lee, R. Thomale, *et al.*, Experimental identification of the second-order non-hermitian skin effect with physics-graph-informed machine learning, *Advanced Science* **9**, 2202922 (2022).

[117] H. Yuan, W. Zhang, Z. Zhou, W. Wang, N. Pan, Y. Feng, H. Sun, and X. Zhang, Non-hermitian topoelectrical circuit sensor with high sensitivity, *Advanced Science* , 2301128 (2023).

[118] D. Zou, T. Chen, H. Meng, Y. S. Ang, X. Zhang, and C. H. Lee, Experimental observation of exceptional bound states in a classical circuit network, *arXiv preprint arXiv:2308.01970* (2023).

[119] P. Zhu, X.-Q. Sun, T. L. Hughes, and G. Bahl, Higher rank chirality and non-hermitian skin effect in a topoelectrical circuit, *Nature communications* **14**, 720 (2023).

[120] H. Zhang, T. Chen, L. Li, C. H. Lee, and X. Zhang, Electrical circuit realization of topological switching for the non-hermitian skin effect, *Physical Review B* **107**, 085426 (2023).

[121] W. Gou, T. Chen, D. Xie, T. Xiao, T.-S. Deng, B. Gadiway, W. Yi, and B. Yan, Tunable nonreciprocal quantum transport through a dissipative aharonov-bohm ring in ultracold atoms, *Physical review letters* **124**, 070402 (2020).

[122] J. M. Koh, T. Tai, and C. H. Lee, Simulation of interaction-induced chiral topological dynamics on a digital quantum computer, *Physical Review Letters* **129**, 140502 (2022).

[123] A. Kirmani, K. Bull, C.-Y. Hou, V. Saravanan, S. M. Saeed, Z. Papić, A. Rahmani, and P. Ghaemi, Probing geometric excitations of fractional quantum hall states on quantum computers, *Physical Review Letters* **129**, 056801 (2022).

[124] P. Frey and S. Rachel, Realization of a discrete time crystal on 57 qubits of a quantum computer, *Science advances* **8**, eabm7652 (2022).

[125] E. Chertkov, Z. Cheng, A. C. Potter, S. Gopalakrishnan, T. M. Gatterman, J. A. Gerber, K. Gilmore, D. Gresh, A. Hall, A. Hankin, *et al.*, Characterizing a non-equilibrium phase transition on a quantum computer, *Nature Physics* , 1 (2023).

[126] T. Chen, R. Shen, C. H. Lee, B. Yang, and R. W. Bomantara, A robust large-period discrete time crystal and its signature in a digital quantum computer, *arXiv preprint arXiv:2309.11560* (2023).

[127] Y. Yang, A. Christianen, S. Coll-Vinent, V. Smelyanskiy, M. C. Bañuls, T. E. O'Brien, D. S. Wild, and J. I. Cirac, Simulating prethermalization using near-term quantum computers, *PRX Quantum* **4**, 030320 (2023).

[128] M. Iqbal, N. Tantivasadakarn, R. Verresen, S. L. Campbell, J. M. Dreiling, C. Figgatt, J. P. Gaebler, J. Johansen, M. Mills, S. A. Moses, *et al.*, Creation of non-abelian topological order and anyons on a trapped-ion processor, *arXiv preprint arXiv:2305.03766* (2023).

[129] R. Shen, T. Chen, B. Yang, and C. H. Lee, Observation of the non-hermitian skin effect and fermi skin on a digital quantum computer, *arXiv preprint arXiv:2311.10143* (2023).

[130] J. M. Koh, T. Tai, and C. H. Lee, Observation of higher-order topological states on a quantum computer, *arXiv preprint arXiv:2303.02179* (2023).

[131] L. Yuan, Y. Shi, and S. Fan, Photonic gauge potential in a system with a synthetic frequency dimension, *Optics letters* **41**, 741 (2016).

[132] F. Klauck, M. Heinrich, and A. Szameit, Photonic two-particle quantum walks in su-schrieffer-heeger lattices, *Photonics Research* **9**, A1 (2021).

[133] R. Umucalilar and I. Carusotto, Artificial gauge field for photons in coupled cavity arrays, *Physical Review A—Atomic, Molecular, and Optical Physics* **84**, 043804 (2011).

[134] M. J. Hartmann, F. G. Brandao, and M. B. Plenio, Quantum many-body phenomena in coupled cavity arrays, *Laser & Photonics Reviews* **2**, 527 (2008).

[135] M. J. Hartmann, F. G. Brandao, and M. B. Plenio, Strongly interacting polaritons in coupled arrays of cavities, *Nature Physics* **2**, 849 (2006).

[136] A. Yariv, Y. Xu, R. K. Lee, and A. Scherer, Coupled-resonator optical waveguide:? a proposal and analysis, *Optics letters* **24**, 711 (1999).

[137] G. Corrielli, A. Crespi, G. Della Valle, S. Longhi, and R. Osellame, Fractional bloch oscillations in photonic lattices, *Nature communications* **4**, 1555 (2013).

[138] S. Longhi, Photonic bloch oscillations of correlated particles, *Optics letters* **36**, 3248 (2011).

[139] L. Feng, Z. J. Wong, R.-M. Ma, Y. Wang, and X. Zhang, Single-mode laser by parity-time symmetry breaking, *Science* **346**, 972 (2014).

[140] B. Peng, S. K. Özdemir, F. Lei, F. Monifi, M. Gianfreda, G. L. Long, S. Fan, F. Nori, C. M. Bender, and L. Yang, Parity-time-symmetric whispering-gallery microcavities, *Nature Physics* **10**, 394 (2014).

[141] L. Chang, X. Jiang, S. Hua, C. Yang, J. Wen, L. Jiang, G. Li, G. Wang, and M. Xiao, Parity-time symmetry and variable optical isolation in active-passive-coupled microresonators, *Nature photonics* **8**, 524 (2014).

[142] F. Zhang, Y. Feng, X. Chen, L. Ge, and W. Wan, Synthetic anti-pt symmetry in a single microcavity, *Physical review letters* **124**, 053901 (2020).

[143] H. Hodaei, M.-A. Miri, M. Heinrich, D. N. Christodoulides, and M. Khajavikhan, Parity-time-symmetric microring lasers, *Science* **346**, 975 (2014).

[144] H. Zhao, P. Miao, M. H. Teimourpour, S. Malzard, R. El-Ganainy, H. Schomerus, and L. Feng, Topological hybrid silicon microlasers, *Nature communications* **9**, 981 (2018).

[145] A. Imamoğlu, H. Schmidt, G. Woods, and M. Deutsch, Strongly interacting photons in a nonlinear cavity, *Physical Review Letters* **79**, 1467 (1997).

[146] I. Carusotto, D. Gerace, H. Tureci, S. De Liberato, C. Ciuti, and A. Imamoğlu, Fermionized photons in an array of driven dissipative nonlinear cavities, *Physical review letters* **103**, 033601 (2009).

- [147] C. Sträter, S. C. Srivastava, and A. Eckardt, Floquet realization and signatures of one-dimensional anyons in an optical lattice, *Physical Review Letters* **117**, 205303 (2016).
- [148] I. Fushman, D. Englund, A. Faraon, N. Stoltz, P. Petroff, and J. Vuckovic, Controlled phase shifts with a single quantum dot, *science* **320**, 769 (2008).
- [149] A. Kubanek, A. Ourjoumtsev, I. Schuster, M. Koch, P. W. Pines, K. Murr, and G. Rempe, Two-photon gateway in one-atom cavity quantum electrodynamics, Physical Review Letters **101**, 203602 (2008).
- [150] M. Koch, C. Sames, M. Balbach, H. Chibani, A. Kubanek, K. Murr, T. Wilk, and G. Rempe, Three-photon correlations in a strongly driven atom-cavity system, *Physical review letters* **107**, 023601 (2011).
- [151] T. Volz, A. Reinhard, M. Winger, A. Badolato, K. J. Hennessy, E. L. Hu, and A. Imamoglu, Ultrafast all-optical switching by single photons, *Nature Photonics* **6**, 605 (2012).